HHS Public Access

Author manuscript

Geoderma. Author manuscript; available in PMC 2024 March 07.

Published in final edited form as:

Geoderma. 2024 February ; 442: . doi:10.1016/j.geoderma.2024.116784.

Understanding the influence of soil development on contaminant reactivity along a fluvial chronosequence in the Oregon Coast Range

Chelsea S. Obeidy[*],

Matthew L. Polizzotto

Department of Earth Sciences, University of Oregon, 100 Cascade Hall, 1272 University of Oregon, Eugene, OR 97403-1272, United States

Abstract

Weathering processes are recognized as drivers of soil and water resource sustainability, but how pedogenesis stage impacts contaminant reactivity and mobility in soils has been minimally investigated. The primary goal of this study was to quantify how soil development influences contaminant reactivity. To achieve this goal, soils from two depths (30 and 100 cm) across a chronosequence (ages 3.5, 20, 69, 140, 200, and 908 ky) in the Oregon Coast Range were subjected to arsenic (As) adsorption isotherms, with As removal from solution serving as a proxy for soil-contaminant reactivity. Langmuir models were applied to isotherm data to quantify relationships between contaminant retention capacity, soil age and soil physicochemical properties, and data revealed that 20 ky soils from a 30-cm-depth had the greatest affinity for As sorption (8,474.5 mg kg^{-1}). Chemical extractions revealed that amorphous (oxy)hydroxides were the dominant mineral phases governing As sorption, even in the presence of abundant crystalline oxides. Micro-X-ray fluorescence spectroscopy revealed a strong spatial correlation between As and Fe in reacted soils. The abundance of amorphous minerals within soils is controlled by the balance between their production from weathering of primary minerals and their loss from ripening to crystalline minerals, and because the mode, extent and minerals governing contaminant sorption determine solid-aqueous phase partitioning, this knowledge will assist in improving models for predicting Critical Zone processes that govern the sustainability of soil and water quality.

[*]Corresponding author. cobeidy@uoregon.edu (C.S. Obeidy).

CRediT authorship contribution statement

Chelsea S. Obeidy: Conceptualization, Data curation, Formal analysis, Investigation, Methodology, Visualization, Writing – original draft, Writing – review & editing. **Matthew L. Polizzotto:** Conceptualization, Project administration, Resources, Supervision, Writing – review & editing.

Declaration of competing interest

The authors declare that they have no known competing financial interests or personal relationships that could have appeared to influence the work reported in this paper.

Appendix A. Supplementary data

A document of supporting information includes 5 data tables demonstrating soil properties (SI Tables 1–3), As sorption Langmuir fit parameters (SI Tables 4 and 5), concentrations of Feo, Fed, Alo, and Ald (SI Figure 1), and Feo:Fed ratios (SI Figure 2). Supplementary data to this article can be found online at https://doi.org/10.1016/j.geoderma.2024.116784.

Keywords

Contaminant sorption; Chronosequence; Oregon Coast Range; Amorphous minerals

1. Introduction

The spatial and temporal heterogeneity of weathering complicate projections of contaminant cycling onto our understanding of water and soil resource sustainability. Weathering proceeds as parent material becomes fractured, ground, dissolved, and bioturbated into chemically altered and potentially transportable materials, processes that can take thousands of years (Buol et al., 2011). At the shortest timescales, chemical reactions taking place at the mineral–water interface can take seconds to minutes, resulting in the ripening of primary minerals, but such processes vary from soil particle (millimeter) to landscape (kilometer) scales (Brantley et al., 2017, 2007; Chorover et al., 2007). Many efforts have been made towards identifying the influences of weathering on Critical Zone (CZ) processes. However, CZ weathering and its influences on reactions that govern contaminant fate and transport are poorly identified and constrained.

Weathering drives the transformation, formation, and accumulation of secondary minerals that are essential for understanding and predicting contaminant reactivity in soils. For instance, weathering releases Fe from primary minerals and governs the generation of secondary Fe oxides, hydroxides, and oxyhydroxides that are dynamic and reactive due to their surface structures, areas, and charges (Bigham et al., 2002; Bowell, 1994; Brown et al., 1999; Duckworth et al., 2022). Secondary Fe minerals and their influence over contaminant reactivity have been the focus of extensive research in pure mineral systems (Dixit and Hering, 2003; Ona-Nguema et al., 2005; Raven et al., 1998). However, when this knowledge is upscaled to the field, reactions that govern the sustainability of soil and water quality are not always consistent due to heterogeneity at various scales within a landscape (Brantley et al., 2007; Hingston et al., 1971; Peel et al., 2022; Smedley and Kinniburgh, 2002; Vitre et al., 1991).

Pedogenic Fe-mineral transformations through weathering and their influence on contaminant sorption have begun to be investigated using chronosequences. In volcanic soils ages 1.5 to 1,070 ky, amorphous Fe phases (denoted ‘Feo’ for their characterization via oxalate-based extractions) have been identified as the dominant hosts for sorption of contaminants, with sorption affinities for copper (Cu) and cadmium (Cd) decreasing with age as Fe-mineral crystallinity and electrical conductivity increased (Rechberger et al., 2020; Rechberger et al., 2021). In contrast, the influence of soil weathering on sorption of dissolved PO_4^{3-} in a young volcanic chronosequence (0.77–1.2 ky) found that sorption increased with soil age, regardless of depth, and was correlated with increasing allophane concentrations (Lilienfein et al., 2004). Within these systems, the underlying mechanistic controls of weathering on contaminant reactivity need to be further identified, particularly for non-volcanic soils.

The present study seeks to examine contaminant reactivity as a function of weathering in nonvolcanic soils. We specifically hypothesized that arsenic (As) sorption would increase

with soil age and depth due to the preponderance of secondary Fe minerals generated through weathering. To test this hypothesis, we harnessed samples from a well-characterized chronosequence in the Oregon Coast Range (OCR) in order to link the influences of weathering on processes that govern contaminant mobility. We sought to quantify (1) arsenic sorption within the OCR as a function of soil age and depth and (2) the dominant host phases governing As sorption as a function of age and depth. Our findings reveal that As sorption onto soils as a function of age and depth did not proceed as initially hypothesized, with amorphous minerals dominating arsenic sorption but the magnitude of sorption varying based on weathering stage. This work highlights the need for understanding the intricacies of weathering-influenced reactions that govern the sustainability of soil and water resources.

2. Materials and methods

2.1. Study site and soil Samples

Soils from a well-characterized fluvial chronosequence were used to elucidate the influence of soil pedogenesis on contaminant reactivity (SI Table 1, SI Table 2) (Almond et al., 2007; Hunter et al., 2023; Lindeburg et al., 2013). Six soil terraces of ages 3.5, 20, 69, 140, 200, and 908 ky were used in this analysis. Soils are derived from the Tyee Formation, a lithified Eocene-aged sandstone-dominated ramp turbidite sequence found in the Coast Range of western Oregon, USA (Fig. 1) (Heller and Dickinson, 1985). The dominant parent material mineralogy of this formation consists of quartz, andesine, calcic andesine, and lithic fragments (Heller et al., 1985; Lindeburg et al., 2013; Ryu, 2003; Snavely et al., 1964). Time-dependent alterations include profile thickness, soil redness, and accumulation of secondary minerals. Pedogenesis within this chronosequence is dominated by the transformation of primary minerals to secondary clays and metal (oxy)hydroxides. Pedogenic Al decreases while Fe increases with terrace age (Fig. 2). Non-quartz Si is either leached or bound in secondary aluminosilicate clays.

Oregon Coast Range soils from 3.5, 20, 69, 140, 200, and 908 ky terraces were used for sorption isotherms, and for all but one terrace, 30- and 100-cm-depth soils were tested; the exception was for the 3.5 ky terrace because soil did not reach 100-cm depth. These samples represent all the characterized terrace ages and depth increments from the target chronosequence (Lindeburg et al., 2013). Soils from each terrace age were used to identify the influence of soil age on sorption capacities, and 30- and 100-cm depths were utilized to identify pedogenic variabilities with depth. Soils were all oven-dried for 48 h at 105 °C and passed through a 2-mm sieve. Amorphous and crystalline Fe and Al were extracted by 0.2 M ammonium acid and oxalic acid buffered at a pH of 3 (McKeague et al., 1971) and citrate-bicarbonate-dithionite (Mehra and Jackson, 1958), respectively. The resulting data are presented in Fig. 2 and SI Table 3, with oxalate extractable designating amorphous Fe and Al (oxy)hydroxide phases, and dithionite extractable designating crystalline Fe and Al (oxy)hydroxide phases (Lindeburg et al., 2013).

2.2. Adsorption isotherms

Arsenic sorption isotherms were conducted to quantify how soil age influenced contaminant reactivity. For each selected soil sample, one gram of soil was mixed with 10 mL of

solution containing one of seven concentrations of As, ranging from 0 to 1,000 mg L^{-1}. Arsenic was added as $Na_2HAsO_4{\cdot}7H_2O$ (Alfa Aesar crystalline powder), and 0.1 M NaCl (VWR Chemicals) was also included in the solutions to maintain ionic strength. pH was maintained at in-situ soil conditions (pH 5 ± 0.2) by HCl or NaOH addition every 24 h. Soil slurries were shaken on a SCI-LOGEX MX-RD-pro shaker at room temperature for 48 h, then centrifuged at 10,000 rpm for 15 min. Soils were then decanted, and resulting solutions were filtered through 1-μm Whatman filter paper before being acidified with one drop of concentrated HNO_3. Solutions were stored in a refrigerator and diluted 100-fold in 2 % HNO_3 for As analysis via inductively coupled plasma-optical emission spectroscopy (ICP-OES) at Oregon State University's Keck Laboratory. The detection limit for As on the Spectros Arcos ICP-OES in side-on view is ~0.05 mg L^{-1}. Starting As sorption solutions were acidified and refrigerated until analysis, along with triplicate soil blanks to ensure quality control. All experiments and analyses were conducted in triplicate.

Data generated from sorption isotherms were used to model As sorption characteristics for each soil sample. Data conformed best to Langmuir models (R^2 = 0.99), and the following equation was used quantify the maximum As sorption capacity (q_{max}) for each soil:

$$\left(q = \frac{K_L C_{eq} q_{max}}{1 + K_L C_{eq}}\right)$$

In this equation, K_L is the Langmuir constant, C_{eq} is equilibrium concentration of As remaining in solution after sorption isotherms, and q is the equilibrium concentration of As (mg kg^{-1}) that sorbed onto soils. The maximum sorption capacity, q_{max}, was derived for each sample and used as a metric for comparison of As sorption capacities across all tested soil samples.

2.3. Chemical extractions

Ammonium oxalate/oxalic acid extractions were conducted to target amorphous phases that served as the host phase for As after sorption incubations. Ammonium oxalate and oxalic acid extracts target As coprecipitated with amorphous Fe and Al (oxy)hydroxides by ligand-promoted dissolution (Keon et al., 2001). Extractions were conducted in triplicate on soils that were dosed with 1,000 mg L^{-1} of As. Soils used for extractions came from 20- and 908-ky soils from a 30- and 100-cm depth, as they represented the most contrasting soils with respect to stage of weathering and arsenic sorption. Soils were air dried after As isotherms, then 0.4 g of soil and 40 mL of 0.2 M ammonium oxalate and oxalic acid solution were placed into 50 mL HDPE centrifuge tubes and vortexed before placing on a shaker. Samples were shaken in the dark on an Orbital Shaker SYC-2102A at room temperature for 2 h. After the 2-h incubation period, samples were centrifuged at 2,000 rpm for 15 min. Solutions were then filtered through 1-μm Whatman filter paper, acidified, and stored in the refrigerator. Samples were then diluted 100-fold in 2 % HNO_3 and analyzed for As on the ICP-OES at Oregon State University. All analyses were conducted in triplicate.

Citrate-bicarbonate-dithionite (CBD) extractions were conducted to target crystalline Fe-(oxy)hydroxides that were associated with As after sorption isotherms (Mehra and Jackson, 1958). Extractions were conducted on 20- and 908-ky soils from 30- and 100-cm depth

that were dosed with 1,000 mg L^{-1} of As and 0.1 NaCl, as previously described. For each sample, 0.4 g of dosed soils were placed into 50 mL HDPE centrifuge tubes along with 20 mL of 0.3 M sodium citrate and 2.5 mL of 1 M sodium bicarbonate. Samples were heated in a hot water bath to 80 °C, then 0.5 g of sodium dithionite were added. Samples were in the hot water bath for 30 min and shaken intermittently, after which, soils were removed and centrifuged at 2,000 rpm for 15 min. Solutions were then filtered using 1-μm Whatman filter paper, preserved with concentrated HNO_3, and stored in the refrigerator until analysis. Samples were diluted 100-fold in 2 % HNO_3 and analyzed for As on the ICP-OES at Oregon State University. All analyses were conducted in triplicate.

2.4. Micro-X-Ray fluorescence imaging

Micro X-ray fluorescence (μ-XRF) elemental mapping was conducted on Beamline 2–3 at the Stanford Synchrotron Radiation Lightsource (SSRL) to identify spatial relationships between As and soil elements. Two soils with contrasting ages and depths were analyzed: 20 ky from a 30-cm-depth and 908 ky from a 100-cm-depth. Soils were dosed with 1,000 mg L^{-1} of As, dried, and then thin-sectioned at Spectrum Petro-graphics. Thin sections were mounted onto quartz glass slides using Epotex-301 resin. μ-XRF mapping was conducted in fluorescence mode using a harmonic rejection mirror and a channel-cut Si(III) mono-chromator. The beam was 2 μm by 2 μm beam size. Elemental maps were created with 7 μm step sizes and 25 ms dwell times at an incident energy of 12 keV. Data were analyzed via Sam's Microprobe Analysis Kit (Webb, 2011).

3. Results

3.1. Adsorption model

The sorption of As onto soils of 30- (Fig. 3a) and 100-cm (Fig. 3b) depths as a function of soil age is presented in Fig. 3. Experimental data conformed to L-curves and were best fit to a Langmuir sorption models ($R^2 > 0.99$). Parameters derived from Langmuir fits are presented in Tables 1 and 2. Variability in As sorption was more apparent across the soils from 30-cm than it was in the 100-cm soils. Langmuir-calculated As sorption maximum (q_{max}) was lowest in the youngest soil (3.5 ky, 30 cm), with a value of 1,666 mg As kg^{-1} but was greatest in the next-youngest soil examined (20 ky, 30 cm), with a value of 8,475 mg As kg^{-1} (Table 1, Fig. 4). As soils got older, calculated q_{max} values clustered from 6,622 to 7,143 mg As kg^{-1} in 30-cm samples. Soils at depth (100 cm) had sorption maxima that were clustered between 5,000–7,900 mg As kg^{-1}, with the greatest As sorption observed with the 200 ky sample (Table 2, Fig. 4).

Maximum As sorption capacity per amorphous and crystalline Fe and Al from 30- and 100-cm soils is presented in Fig. 5. Concentrations of Feo, Fed, Alo, and Ald, indicative of amorphous and crystalline Fe and Al, were provided by Lindeburg et al. (2013) and summed. Arsenic sorption per Fe and Al-phases in 30- and 100-cm soils decreased with soil age, from 1,549 to 870 mg kg^{-1}. The highest As sorption per Fe and Al phases was in 20-ky soils from a 100-cm depth and the lowest sorption was in 200-ky soils from a 100-cm depth. Arsenic sorption per Fe and Al phases decreased more rapidly in soils from a 100-cm depth than from 30-cm depth, and both soil depths remained relatively consistent in As

sorption capacities between 200 and 908 ky. Arsenic sorption per Fe and Al was relatively consistent in soils from 30-cm depth 3.5 to 20 ky and then gradually decreased with soil age. In 100-cm soils, As sorption per Fe and Al decreased substantially between 20- and 200-ky soils, and thereafter, As sorption decreased minimally with soil age.

3.2. Arsenic host phases

Chemical extractions revealed that after incubation of 1,000 mg L^{-1} As solution, amorphous materials (ammonium oxalate and oxalic acid extractable) were the dominant host-phases of sorbed As (Fig. 6). The highest concentration of As extracted was from oxalate extractions in 20-ky soils from a 30-cm depth (4,842.7 mg kg^{-1}), followed by 20-ky soils from a 100-cm depth (3,781.6 mg kg^{-1}); these soils sorbed 64–69 % of As from solution. Oxalate extractions of As-doped, 908-ky soils from 30- and 100-cm-depth yielded 1,736.3 mg kg^{-1} and 1,786.5 mg kg^{-1} of As, respectively, indicating that 27–31 % of added As sorbed to amorphous phases. Citrate-bicarbonate-dithionite extractions, indicative of As sorbed to crystalline oxide phases, yielded less As than all oxalate extractions, with As extracted ranging from 215.1 mg kg^{-1} (908 ky, 100-cm-depth) to 724.2 mg kg^{-1} (20 ky, 30-cm depth).

Micro X-ray fluorescence (μ-XRF) analyses revealed that As was strongly associated with Fe in both 20-ky, 30-cm-depth soil and 908-ky, 100-cm-depth soil (Fig. 7). In 20 ky soils, As was less homogenously associated with Fe and there were more independent zones of As whereas As sorption in 908 ky soil was more homogenously associated with Fe, reflected by the slightly higher R^2 values quantifying spatial correlation between the elements (0.99 for 908-ky soil and 0.91 for 20-ky soil).

4. Discussion

4.1. Progression of soil weathering

Soil weathering in the OCR chronosequence is dominated by the conversion of primary minerals into secondary minerals and oxides. The percentage of oxalate-extractable Fe in soils minimally varies with age and depth (0.32—1.25 % oxalate-extractable Fe); the highest concentration was in 20 ky soils from a 30-cm depth while the lowest was in 908 ky soils from a 30-cm depth (Fig. 2). Except for 908 ky soils, all soils had higher concentrations of oxalate-extractable Fe at a 30-cm depth than at 100-cm depth (Fig. 2). Relatively stable concentrations of oxalate-extractable Fe that persist in soils throughout pedogenesis are maintained by a balance between the rates of Fe weathering from primary minerals to amorphous oxides (oxalate extractable) and the ripening from amorphous to crystalline Fe-oxide phases (dithionite extractable). Dithionite-extractable Fe concentrations in OCR soils increase with soil age from ~0.5 to 6 % Fe. Between 200 ky and 908 ky, soils at depth (100 cm) appear to reach steady-state concentrations of dithionite-extractable Fe, which is likely limited by primary mineral weathering rates (Fig. 2), although Feo:Fed decreases (SI Fig. 2). Aluminum varied minimally with pedogenesis and at depth; oxalate-extractable Al (0.21–1.56 %) and dithionite-extractable Al (0.18–1.37 %) were highest in soils from a 30-cm-depth. Between 3.5 and 20 ky, soils increase in oxalate- and dithionite-extractable Al, which is likely indicative of the ripening of primary Al-minerals (Fig. 2).

The development of secondary oxides within the OCR chronosequence is consistent with the general model of pedogenesis in non-volcanic soils. Oxalate-extractable Fe concentrations are highest in moderately young soils and slightly decrease with soil age and depth (McFadden and Hendricks, 1985). Accumulation of dithionite-extractable Fe from 69 to 200 ky in OCR soils is consistent with other chronosequences, where the increasing dithionite-extractable Fe was observed from 105 to 490 ky and was attributed to the release of the Fe-containing primary minerals through weathering (Fig. 2) (Lawrence et al., 2015; Schulz et al., 2010). After the rapid accumulation of dithionite-extractable Fe, steady-state concentrations are reached due to exhumation of primary Fe-bearing minerals; in OCR soils, this was observed between 200 and 908 ky, and this has been reported in other chronosequences between 300 and 600 ky (Fig. 2)(Aniku and Singer, 1990).

4.2. Arsenic sorption as a function of soil age and depth

The rates of weathering and generation of amorphous-secondary minerals ultimately govern contaminant fate in the subsurface environment. We initially hypothesized that the preponderance of Fe-oxide minerals present in OCR soils would result in increased As sorption with soil age and with depth. However, contrary to our hypothesis, we did not observe a correlation between soil age and As sorption maxima but rather, As sorption per (oxy)hydroxide Fe and Al (oxalate- and CBD-extractable Fe) decreased through pedogenesis after 3.5 ky (Fig. 5). Although crystalline Fe- and Al-oxide phases are well-established sorbents for As (Giménez et al., 2007; Grafe et al., 2001; Ladeira and Ciminelli, 2004; Mamindy-Pajany et al., 2009; Smedley and Kinniburgh, 2002), oxalate-extractable phases, indicative of amorphous Fe-oxide and possibly amorphous Al-oxide phases, disproportionately influenced contaminant sorption in our samples, regardless of soil age and depth. Comparing samples from different depths, 30-cm soils had a higher affinity for As sorption than 100-cm soils until 200 ky, after which trends reversed (Fig. 3).

Previous studies that have investigated the influences of weathering on contaminant reactivity have observed peak sorption maxima at a younger stage of pedogenesis than what was observed in the OCR soils. In volcanic soils, contaminant sorption is highest at an earlier stage of pedogenesis (1.2—1.5 ky), while OCR soils reached maximum sorption in 20 ky soils (Fig. 3) (Lilienfein et al., 2004; Rechberger et al., 2020; Rechberger et al., 2021). In these studies, soil sorption maxima of Cd and Cu decreased with increased soil weathering (Rechberger et al., 2020; Rechberger et al., 2021). The delayed maximum sorption affinities in OCR soils are likely due to differences in volcanic and non-volcanic parent material weathering rates; poorly crystalline volcanic parent materials weather more rapidly and generate higher concentrations of amorphous materials that have been linked to increased contaminant reactivity at early stages of pedogenesis (Buol et al., 2011; Shoji et al., 1993). Our results highlight the delayed generation of oxalate-extractable minerals in non-volcanic soils that disproportionately influence contaminant reactivity.

4.3. Factors governing arsenic sorption

Chemical extractions revealed that the dominant host-phase of As was the oxalate-extractable fraction in all soils, regardless of age or depth (Fig. 6) and μ-XRF imaging revealed a strong spatial correlation between As and Fe (Fig. 7). Arsenic, as arsenate, has

a high sorption affinity for secondary Fe-minerals and sorbs as an inner-sphere complex (Smedley and Kinniburgh, 2002; Strawn et al., 2015). Arsenate sorption onto oxalate-extractable Fe-minerals, such as ferrihydrite, has been thoroughly investigated because of the mineral's high surface area and affinity for contaminant sorption (Jain et al., 1999; Vitre et al., 1991; Waychunas et al., 1996; Wilkie and Hering, 1996). In pure mineral studies, ferrihydrite can sorb ~3.02 mol of As(V) per kg^{-1} of Fe at pH 4.6 to 5 (Grafe et al., 2002, 2001; Ladeira and Ciminelli, 2004; Raven et al., 1998) whereas crystalline phases of Fe, such as goethite, sorb 0.33 mol of As(V) per kg^{-1} Fe (Grafe et al., 2001). Though As sorbs as inner-sphere complexes in both cases, differences in Fe-oxide surface area influence sorption capacities, as ferrihydrite's surface area can range from 100 to 700 $m^2\ g^{-1}$ whereas goethite and hematite have surface areas ranging from 6 to 115 $m^2\ g^{-1}$ (Barron et al., 1988; Bigham et al., 2002; Cornell and Schwertmann, 2003; Torrent et al., 1990). Although μ-XRF imaging highlights the strong positive correlation between As and Fe and chemical extractions revealed a strong dependence on amorphous phases (Fig. 6, Fig. 7), extrapolating measurements from pure systems to experiments with natural materials is complicated by confounding factors, and in our study, it is probable that aluminum oxides and organic carbon, among other soil components that wouldn't be detectable by the μ-XRF techniques employed, may have also contributed to As sorption at given soil properties and experimental conditions (Manning and Goldberg, 1997; Smedley and Kinniburgh, 2002; Vitre et al., 1991).

Based on measured concentrations of oxalate- and dithionite-extractable Fe and Al in the OCR soils, as well as published As sorption capacity values for pure Fe and Al oxides, we calculated the maximum As sorption we would expect for the OCR soils. To approximate As(V) sorption onto amorphous Fe- and Al-minerals (oxalate-extractable) sorption capacities of ferrihydrite or allophane were used, and based on OCR concentrations of oxalate-extractable Fe and Al, we expect the range of As sorption to be between 0.016 and 0.085 mol of As sorbed to ferrihydrite and allophane per kg^{-1} of soil (Table 3) (Arai et al., 2005; Raven et al., 1998). These calculated values were well matched to our measured values of oxalate-extracted As from As-doped soils (Fig. 6), which ranged from 0.02 to 0.06 mol of oxalate-extractable As kg^{-1} OCR soil. In order to estimate As(V) sorption onto crystalline Fe- and Al-minerals (CBD extractable), goethite and gibbsite's sorption maxima were used, and sorption capacities were expected to range from 0.002 to 0.022 mol of As sorbed to goethite and gibbsite per kg^{-1} of soil (Table 3) (Grafe et al., 2001; Ladeira and Ciminelli, 2004). Measured citrate-bicarbonate-dithionite-extractable As from OCR soils (20 and 908 ky soils from a 30- and 100-cm depth; Fig. 6) overlapped on the lower end of these calculated values, ranging from 0.002 to 0.009 mol of CBD-extractable As kg^{-1} OCR soils.

The expected sorption capacity of As(V) onto oxalate- and dithionite-extractable Fe- and Al-minerals ranged from 0.018 to 0.096 mol of As sorbed to ferrihydrite, allophane, goethite, and gibbsite per kg^{-1} of soil, while maximum As sorption capacities in OCR soils, as determined by Langmuir q_{max} values from our measured isotherms, ranged from 0.022 – 0.113 mol As per kg^{-1} of OCR soil (Fig. 8). In general, sorption capacities observed in OCR soil isotherms were higher than those calculated from pure minerals, which may be attributed to pedogenic ferrihydrite having a greater capacity for As sorption than synthesized ferrihydrite, additional phases–such as organic matter–contributing to As

sorption, and the overall heterogeneity of soils vs. pure mineral systems (Dzombak and Morel, 1991; Hingston et al., 1971; Pierce and Moore, 1982; Smedley and Kinniburgh, 2002; Vitre et al., 1991). Still, the order-of-magnitude agreement of measured As sorption maxima with values calculated from As sorption capacities to pure minerals highlights, in this case, a particularly strong connection between measurements from idealized and field samples.

In general, measured (Fig. 6) and calculated (Table 3) As sorption onto oxalate-extractable phases was frequently over 10 times the As sorption to CBD-extractable phases, which highlights the disproportionate influence of amorphous phases over crystalline phases in governing contaminant sorption. Moreover, differences in phases controlling As sorption, as demonstrated by oxalate vs. CBD extractions, demonstrate how stage of pedogenesis, which creates different quantities and ratios of amorphous and crystalline phases, is a critical driver of contaminant reactivity.

Amorphous Fe and Al concentrations that ultimately govern contaminant mobility in OCR soils are maintained by the rates of primary mineral weathering and the proportion that are transformed towards crystalline-oxide phases (Bigham et al., 2002; Hingston et al., 1971; Smedley and Kinniburgh, 2013). Crystalline Fe- and Al-oxide minerals sorb contaminants by an order of magnitude lower than their amorphous precursors. Our findings suggest that the concentration of amorphous phases, which can be in a roughly steady state balanced by rates of their production from primary mineral weathering and ripening-driven destruction, is the key factor controlling contaminant retention, and this value is therefore critical for assessing contaminant availability and threats to environmental quality within a given soil system. Future research should be directed towards understanding Fe- and Al-oxide genesis in varying soil forming conditions and environments that ultimately govern contaminant reactivity in the subsurface.

5. Conclusion

Soil weathering processes influence the sustainability and quality of soil and water resources in the environment. In using As removal from solution as a proxy for soil-contaminant reactivity in soils from a chronosequence in the Oregon Coast Range (3.5 to 908 ky from a 30- and 100-cm depth) we highlight the strong dependence on short-range-order minerals that disproportionally govern contaminant fate in our environment. Chemical extractions and μ-XRF spectroscopy revealed the strong dependence on amorphous solid-host phases and the strong spatial correlation between As and Fe, respectively. Arsenic sorption capacities are most greatly governed by the concentrations of amorphous (oxy)hydroxide mineral phases, even when crystalline oxides and oxyhydroxide minerals are abundant. The concentration of amorphous minerals is balanced by rates of their production from weathering of primary minerals and rates of loss from ripening to more crystalline phases, which accumulate through pedogenesis. This knowledge can assist in improving models for predicting CZ processes that govern the sustainability of soil and water quality, and future work could aim to understand the influences of different environments on soil weathering, in order to ultimately determine contaminant fate in the environment.

Supplementary Material

Refer to Web version on PubMed Central for supplementary material.

Acknowledgments

We thank Markus Koeneke, Fatai Balogun, Katie Fisher, and Jason John for support in developing and conducting this research; Josh Roering for the chronosequence soils; Owen Duckworth and Sam Webb for assistance in gathering μ-XRF data at the Stanford Synchrotron Radiation Lightsource; and Chris Russo and Jesse Muratli at Oregon State University for assistance in gathering ICP-OES data.

Sources of financial support

This work was supported by the National Institute of Health through the National Institute of Environmental Health Sciences under Grant No. NIH-5P42ES031007-02 and the University of Oregon. Use of the Stanford Synchrotron Radiation Lightsource, SLAC National Accelerator Laboratory, is supported by the U.S. Department of Energy, Office of Science, Office of Basic Energy Sciences under Contract No. DE-AC02-76SF00515.

Data availability

Data will be made available on request.

References

Almond P, Roering J, Hales TC, 2007. Using soil residence time to delineate spatial and temporal patterns of transient landscape response. J. Geophys. Res. Earth Surf 112 10.1029/2006JF000568.

Aniku JRF, Singer MJ, 1990. Pedogenic Iron Oxide Trends in a Marine Terrace Chronosequence. Soil Sci. Soc. Am. J 54, 147–152. 10.2136/sssaj1990.03615995005400010023x.

Arai Y, Sparks DL, Davis JA, 2005. Arsenate adsorption mechanisms at the allophane - Water interface. Environ. Sci. Tech 39, 2537–2544. 10.1021/es0486770.

Barron V, Herruzo M, Torrent J, 1988. Phosphate Adsorption by Aluminous Hematites of Different Shapes. Soil Sci. Soc. Am. J 52, 647–651. 10.2136/sssaj1988.03615995005200030009x.

Bigham JM, Fitzpatrick RW, Schulze DG, 2002. Chapter 10 Iron Oxides. Soil Mineralogy with Environmental Applications. 323–376.

Bowell RJ, 1994. Sorption of arsenic by iron oxides and oxyhydroxides in soils. Appl. Geochem 9, 279–286. 10.1016/0883-2927(94)90038-8.

Brantley SL, Goldhaber MB, Vala Ragnarsdottir K, 2007. Crossing disciplines and scales to understand the critical zone. Elements 3, 307–314. 10.2113/gselements.3.5.307.

Brantley SL, McDowell WH, Dietrich WE, White TS, Kumar P, Anderson SP, Chorover J, Ann Lohse K, Bales RC, Richter DD, Grant G, Gaillardet J, 2017. Designing a network of critical zone observatories to explore the living skin of the terrestrial Earth. Earth Surf. Dyn 5, 841–860. 10.5194/esurf-5-841-2017.

Brown GE, Foster AL, Ostergren JD, 1999. Mineral surfaces and bioavailability of heavy metals: A molecular-scale perspective.

Buol SW, Southard RJ, Graham RC, McDaniel PA, 2011. Soil Genesis and Classification, Sixth. ed. Wiley-Blackwell.

Chorover J, Kretzschmar R, Garcia-pichel F, Sparks DL, 2007. Soil Biogeochemical Processes within the Critical Zone. Elements 3, 321–326.

Cornell RM, Schwertmann U, 2003. The Iron Oxides. Wiley. 10.1002/3527602097.

Dixit S, Hering JG, 2003. Comparison of arsenic(V) and arsenic(III) sorption onto iron oxide minerals: Implications for arsenic mobility. Environ. Sci. Tech 37, 4182–4189. 10.1021/es030309t.

Duckworth OW, Polizzotto ML, Thompson A, 2022. tackle soil contaminants. 10.3389/fenvs.2022.981607.Bringing.

Dzombak D, Morel F, 1991. Surface Complexation Modeling: Hydrous Ferric Oxide. John Wiley, New York.

Giménez J, Martínez M, de Pablo J, Rovira M, Duro L, 2007. Arsenic sorption onto natural hematite, magnetite, and goethite. J. Hazard. Mater 141, 575–580. 10.1016/j.jhazmat.2006.07.020. [PubMed: 16978766]

Grafe M, Eick MJ, Grossl PR, 2001. Adsorption of Arsenate (V) and Arsenite (III) on Goethite in the Presence and Absence of Dissolved Organic Carbon. Soil Sci. Soc. Am. J 65, 1680–1687. 10.2136/sssaj2001.1680.

Grafe M, Eick MJ, Grossl PR, Saunders AM, 2002. Adsorption of Arsenate and Arsenite on Ferrihydrite in the Presence and Absence of Dissolved Organic Carbon. Environmental Quality 1123, 1115–1123.

Heller PL, Dickinson WR, 1985. Submarine ramp facies model for delta-fed, sand-rich turbidite systems. Am. Assoc. Pet. Geol. Bull; (United States) 69: 6.

Heller PL, Peterman ZE, O'Neil JR, Shafiqullah M, 1985. Isotopic provenance of sandstones from the Eocene Tyee Formation, Oregon Coast Range. Geol. Soc. Am. Bull 96, 770–780. 10.1130/0016-7606(1985)96<770:IPOSFT>2.0.CO;2.

Hingston FJ, Posner AM, Quirk JP, Hpoi-, +, 1971. Competitive Adsorption of Negatively Charged Ligands on Oxide Surfaces.

Hunter BD, Roering JJ, Almond PC, Chadwick OA, Polizzotto ML, Silva LCR, 2023. Pedogenic pathways and deep weathering controls on soil organic carbon in Pacific Northwest forest soils. Geoderma 436. 10.1016/j.geoderma.2023.116531.

Jain A, Raven KP, Loeppert RH, 1999. Arsenite and arsenate adsorption on ferrihydrite: Surface charge reduction and net OH-release stoichiometry. Environ. Sci. Tech 33, 1179–1184. 10.1021/es980722e.

Keon NE, Swartz CH, Brabander DJ, Harvey C, Hemond HF, 2001. Validation of an arsenic sequential extraction method for evaluating mobility in sediments. Environ. Sci. Tech 35, 2778–2784. 10.1021/es001511o.

Ladeira ACQ, Ciminelli VST, 2004. Adsorption and desorption of arsenic on an oxisol and its constituents. Water Res. 38, 2087–2094. 10.1016/j.watres.2004.02.002. [PubMed: 15087189]

Lawrence CR, Harden JW, Xu X, Schulz MS, Trumbore SE, 2015. Long-term controls on soil organic carbon with depth and time: A case study from the Cowlitz River Chronosequence, WA USA. Geoderma 247–248, 73–87. 10.1016/j.geoderma.2015.02.005.

Lilienfein J, Qualls RG, Uselman SM, Bridgham SD, 2004. Adsorption of Dissolved Organic and Inorganic Phosphorus in Soils of a Weathering Chronosequence. Soil Sci. Soc. Am. J 68, 620–628. 10.2136/sssaj2004.6200.

Lindeburg KS, Almond P, Roering JJ, Chadwick OA, 2013. Pathways of soil genesis in the Coast Range of Oregon, USA. Plant and Soil 367, 57–75. 10.1007/s11104-012-1566-z.

Mamindy-Pajany Y, Hurel C, Marmier N, Roméo M, 2009. Arsenic adsorption onto hematite and goethite. C. R. Chim 12, 876–881. 10.1016/j.crci.2008.10.012.

McFadden LD, Hendricks DM, 1985. Changes in the content and composition of pedogenic iron oxyhydroxides in a chronosequence of soils in southern California. Quat. Res 23, 189–204. 10.1016/0033-5894(85)90028-6.

McKeague JA, Brydon JE, Miles NM, 1971. Differentiation of Forms of Extractable Iron and Aluminum in Soils. Soil Sci. Soc. Amer. Proc 35, 33–38. 10.2136/sssaj1971.03615995003500010016x.

Mehra OP, Jackson ML, 1958. Iron Oxide Removal from Soils and Clays by a Dithionite-Citrate System Buffered with Sodium Bicarbonate. Clays Clay Miner. 7, 317–327. 10.1346/ccmn.1958.0070122.

Ona-Nguema G, Morin G, Juillot F, Calas G, Brown GE, 2005. EXAFS analysis of arsenite adsorption onto two-line ferrihydrite, hematite, goethite, and lepidocrocite. Environ. Sci. Tech 39, 9147–9155. 10.1021/es050889p.

Peel HR, Balogun FO, Bowers CA, Miller CT, Obeidy CS, Polizzotto ML, Tashnia SU, Vinson DS, Duckworth OW, 2022. Towards Understanding Factors Affecting Arsenic, Chromium, and Vanadium Mobility in the Subsurface. Water (switzerland) 14, 1–36. 10.3390/w14223687.

Pierce ML, Moore CB, 1982. Adsorption of arsenite and arsenate on amorphous iron hydroxide, Dater Res.

Raven KP, Jain A, Loeppert RH, 1998. Arsenite and arsenate adsorption on ferrihydrite: Kinetics, equilibrium, and adsorption envelopes. Environ. Sci. Tech 32, 344–349. 10.1021/es970421p.

Rechberger MV, Zehetner F, Candra IN, Gerzabek MH, 2020. Impact of soil development on Cu sorption along gradients of soil age and moisture on the Galápagos Islands. Catena (amst) 189, 104507. 10.1016/j.catena.2020.104507.

Rechberger MV, Roberti D, Phillips A, Zehetner F, Keiblinger KM, Kandeler E, Gerzabek MH, 2021. Cadmium retention and microbial response in volcanic soils along gradients of soil age and climate on the Galápagos Islands. J. Environ. Qual 50, 1233–1245. 10.1002/jeq2.20275. [PubMed: 34350988]

Ryu I-C, 2003. Petrography, diagenesis and provenance of Eocene Tyee Basin sandstones, southern Oregon Coast Range: New view from sequence stratigraphy. Island Arc 12, 398–410.

Schulz MS, Vivit D, Schulz C, Fitzpatrick J, White A, 2010. Biologic Origin of Iron Nodules in a Marine Terrace Chronosequence, Santa Cruz, California. Soil Sci. Soc. Am. J 74, 550–564. 10.2136/sssaj2009.0144.

Shoji S, Dahlgren R, Nanzyo M, 1993. Chapter 3 Genesis of Volcanic Ash Soils. Developments in Soil Science 21, 37–71. 10.1016/S0166-2481(08)70264-2.

Smedley PL, Kinniburgh DG, 2002. A review of the source, behaviour and distribution of arsenic in natural waters. Appl. Geochem 10.1016/S0883-2927(02)00018-5.

Snavely P, Wagner H, MacLeod N, 1964. Rhythmic-bedded Eugeosynclinal Deposits of the Tyee Formation, Oregon Coast Range. Merriam DF, ed., Kansas Geological Survey 461–480.

Strawn DG, Bohn HL, O'Connor GA, 2015. Soil Chemistry. John Wiley & Sons Ltd.

Torrent J, Barrón V, Schwertmann U, 1990. Phosphate Adsorption and Desorption by Goethites Differing in Crystal Morphology. Soil Sci. Soc. Am. J 54, 1007–1012. 10.2136/sssaj1990.03615995005400040012x.

Vitre RD, Belzile N, Tessier A, 1991. Speciation and adsorption of arsenic on diagenetic iron oxyhydroxides. Limnol. Oceanogr 10.4319/lo.1991.36.7.1480.

Waychunas GA, Fuller CC, Rea BA, Davis JA, 1996. Wide angle X-ray scattering (WAXS) study of "two-line" ferrihydrite structure: Effect of arsenate sorption and counterion variation and comparison with EXAFS results. Geochim. Cosmochim. Acta 60, 1765–1781. 10.1016/0016-7037(96)89830-9.

Webb SM, 2011. The MicroAnalysis Toolkit: Fluorescence Image Processing Software. 10.1063/1.3625338.

Wilkie JA, Hering JG, 1996. Adsorption of arsenic onto hydrous ferric oxide: effects of adsorbate/adsorbent ratios and co-occurring solutes. Colloids Surf. 107, 97–110.

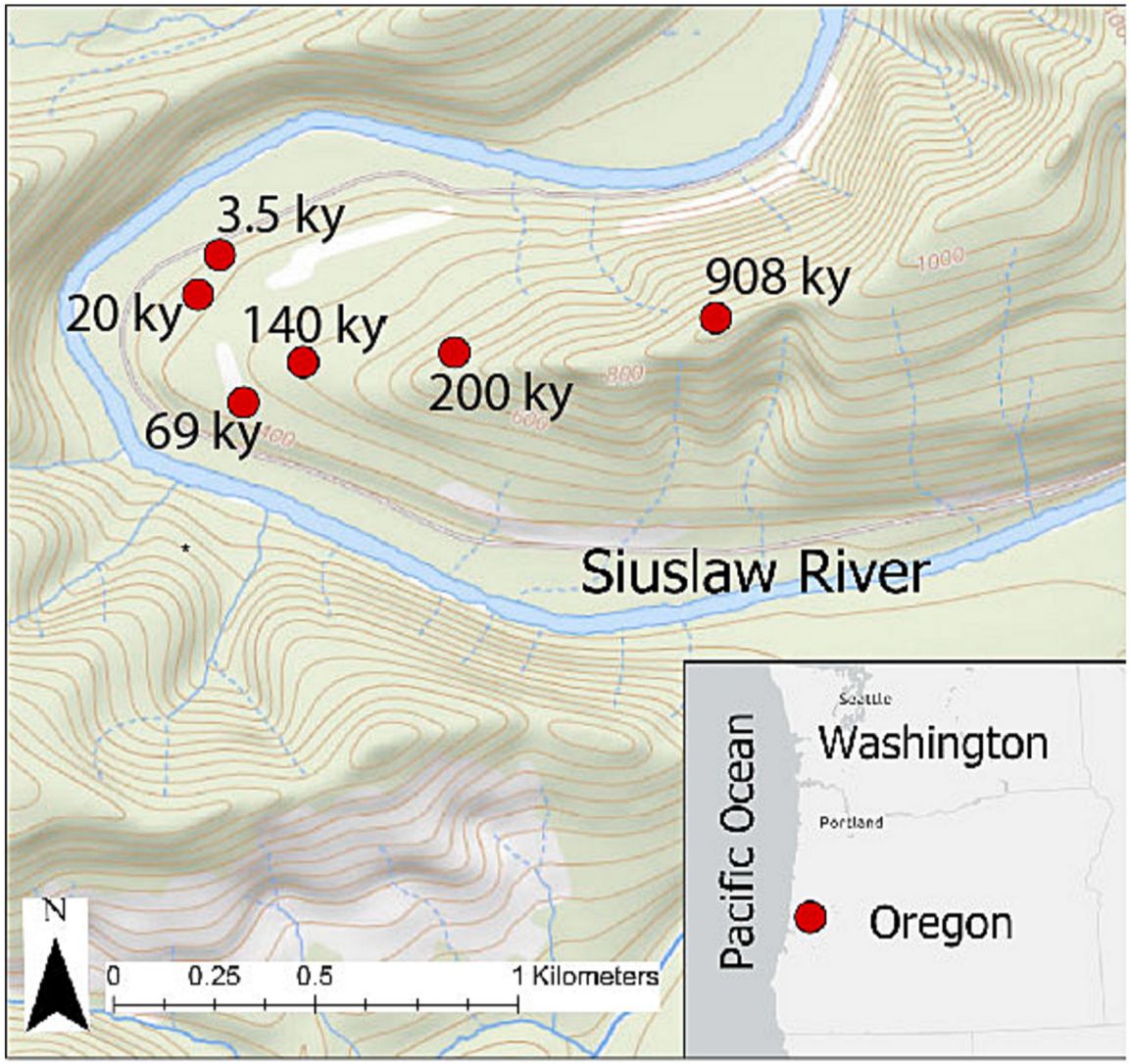

Fig. 1.

Location of fluvial chronosequence analyzed along the Siuslaw river in the Siuslaw National Forest in western Oregon, USA. Soils range in age from 3.5 ky to 908 ky and elevation varies by 163 m (Almond et al., 2007; Hunter et al., 2023; Lindeburg et al., 2013).

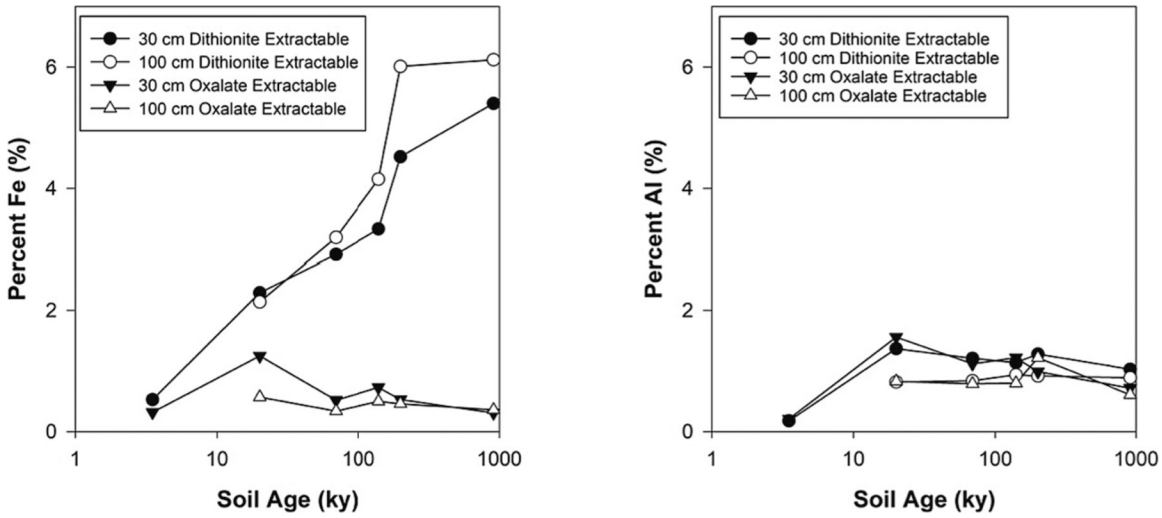

Fig. 2.

(Left) Percent of dithionite-extractable and oxalate-extractable Fe from 30- and 100-cm depth in OCR soils. (Right) Percent of dithionite extractable and oxalate extractable Al from 30- and 100-cm depth in OCR soils. Data were obtained from (Lindeburg et al., 2013).

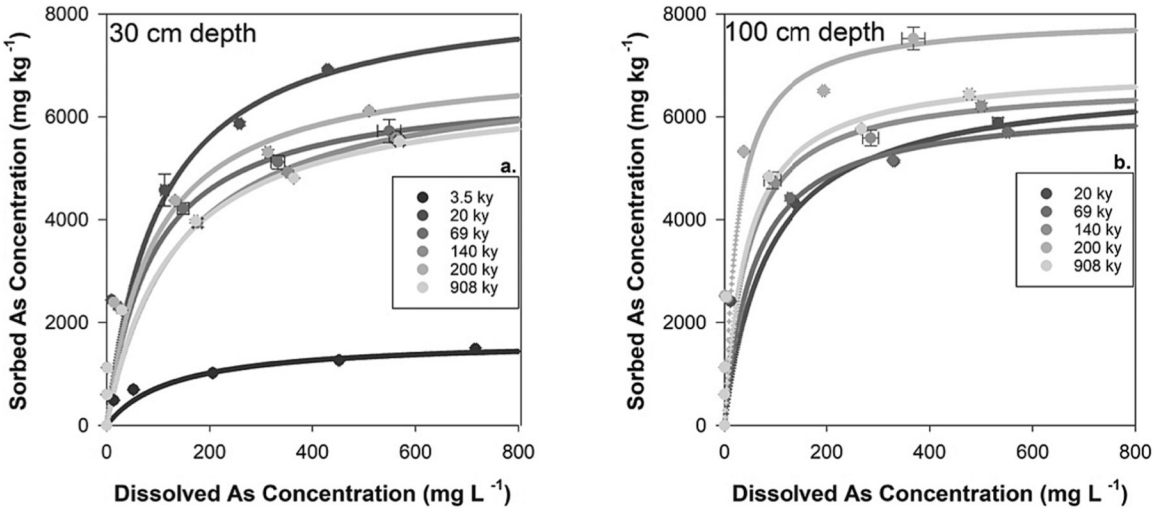

Fig. 3.

Experimental data (symbols) and Langmuir models (lines) of As sorption in varying aged soils from two depths, 30 (3a) and 100 (3b) cm. Soils were incubated in 0–1,000 mg L^{-1} As solution. Experimental data is averaged from triplicate samples and standard error is calculated from triplicate samples.

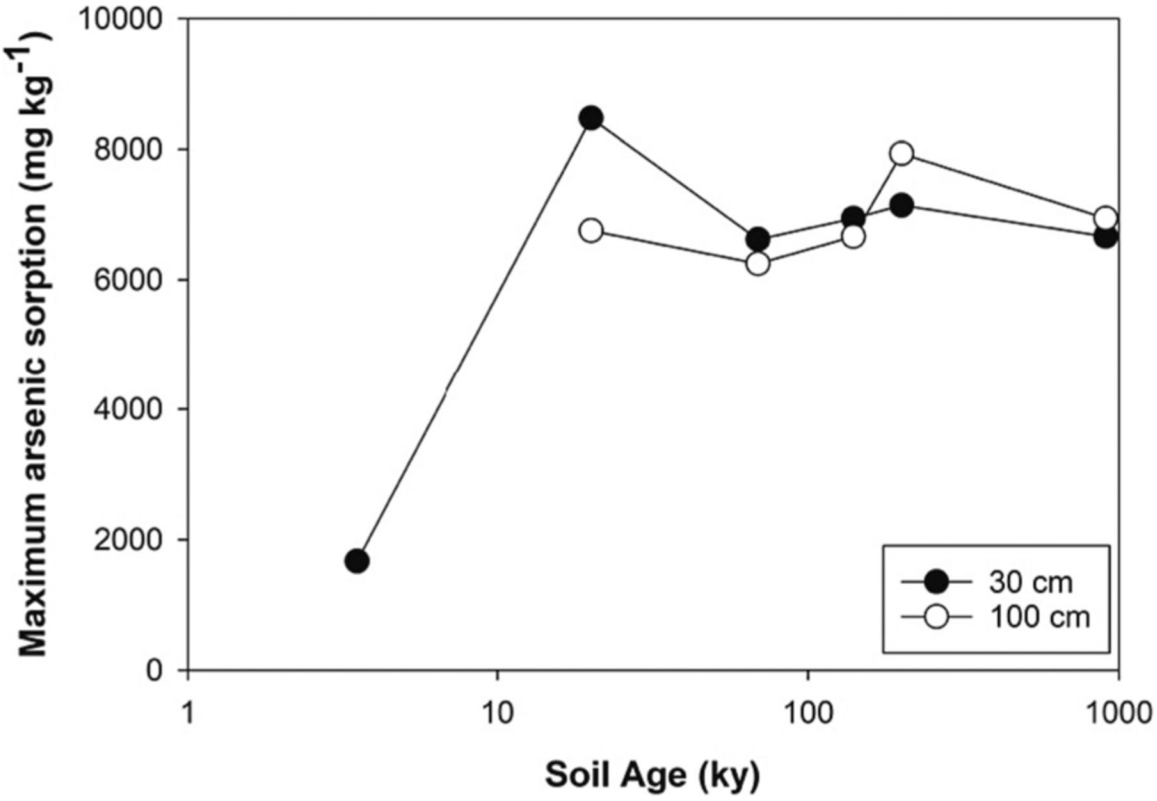

Fig. 4.

Arsenic sorption maxima (q_{max}) as a function of soil terrace age from 30- (black symbols) and 100-cm (white symbols) soils. Maximum capacity for As sorption (q_{max}) was calculated using experimental data and the Langmuir model.

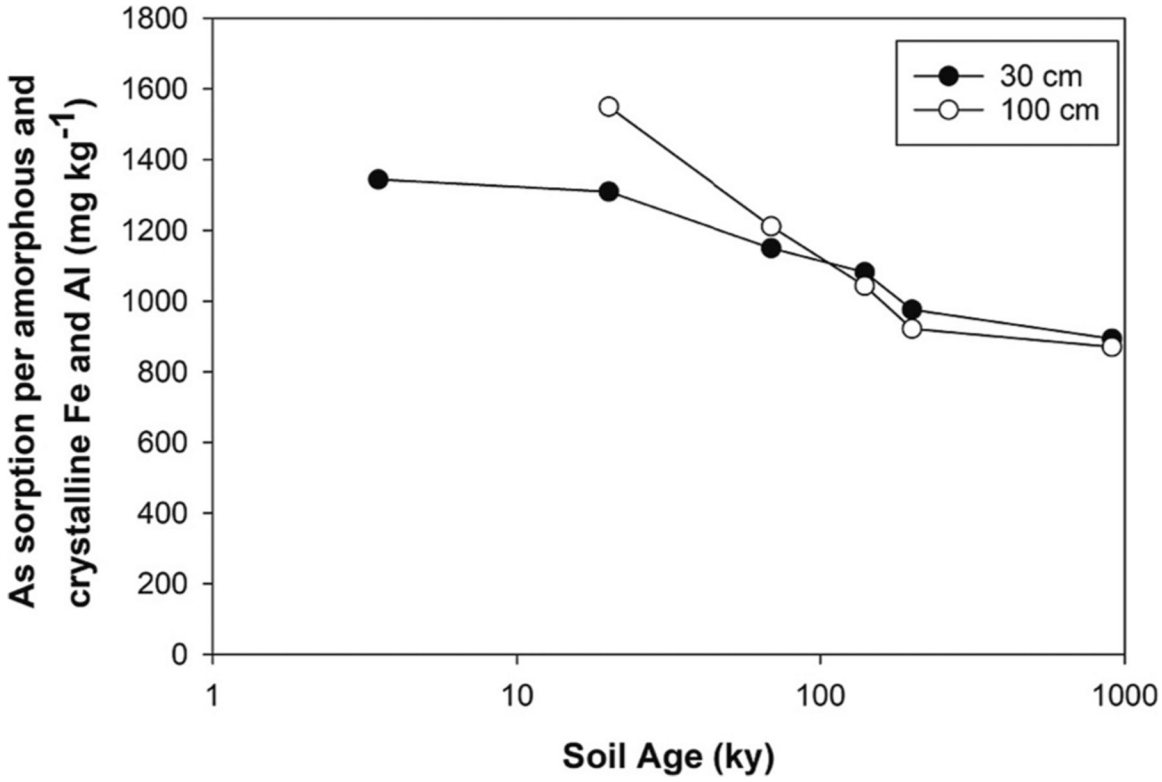

Fig. 5.

Maximum As sorption per amorphous (Feo and Alo) and crystalline (Fed and Ald) phases in 30- and 100-cm soils from the OCR chronosequence. Concentrations of Feo, Fed, Alo, and Ald were provided by Lindeburg et al., 2013.

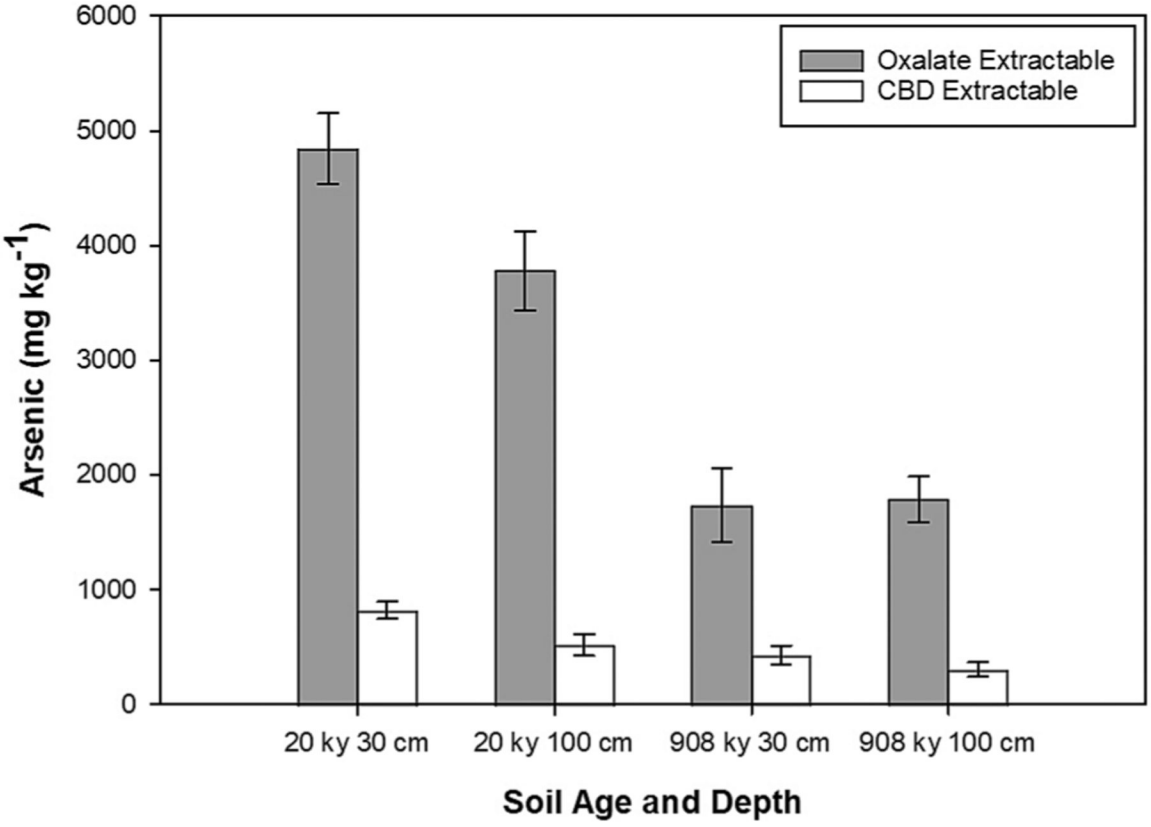

Fig. 6.

Concentrations of oxalate- and CBD-extractable As. Extractions were conducted on soils that were 20- and 908-ky old, from both 30- and 100-cm depths. Soils were dosed with 1,000 mg L^{-1} As for 48 h prior to extractions. Error bars represent standard error of experimental triplicates.

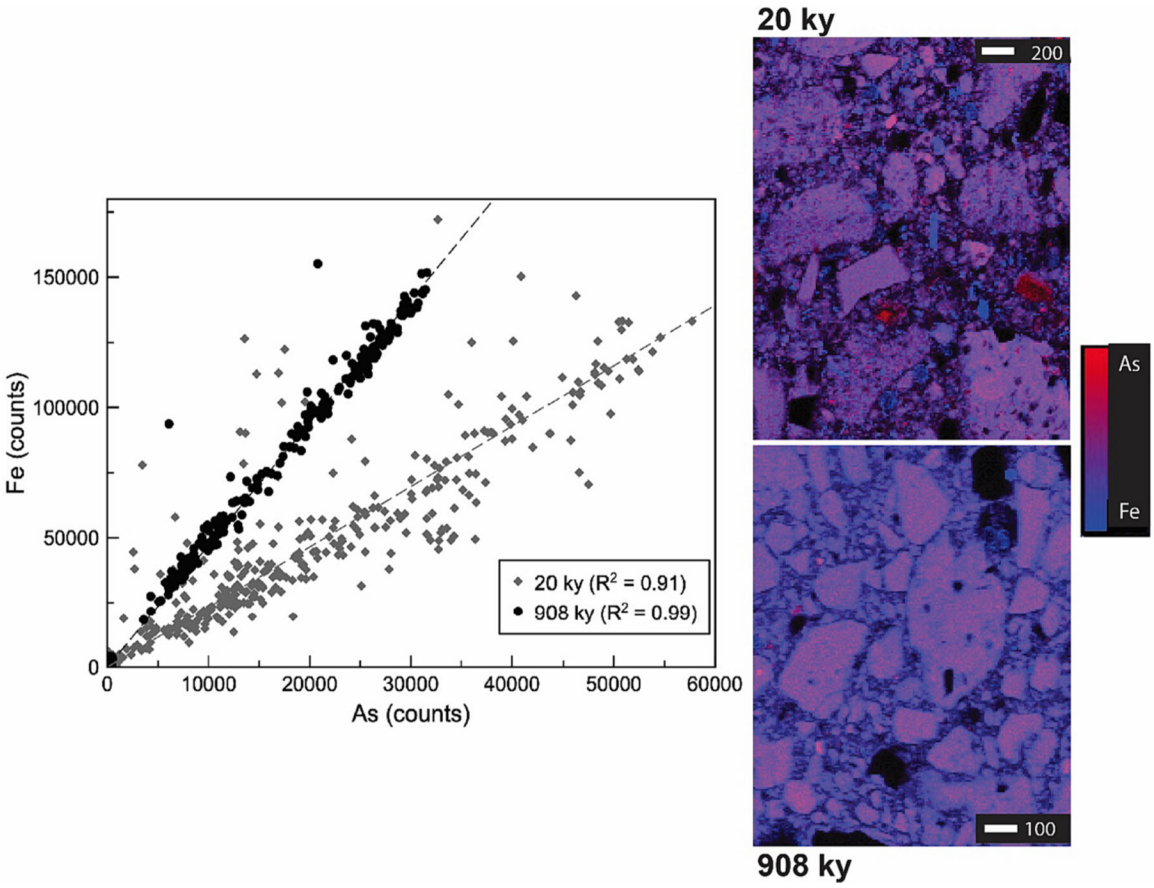

Fig. 7.

Solid phase bicolor elemental maps and correlation plot based on counts of As and Fe obtained from μ-X-ray fluorescence elemental mapping of OCR soils dosed with As. Left: As-Fe spatial correlation plots; grey diamonds represent 20-ky soils from 30-cm-depth and black circles represent 908-ky soils from 100-cm-depth. Right: As and Fe elemental distribution maps; 20-ky (top) and 908-ky (bottom) soils, with red and blue coloration representing As and Fe counts, respectively.

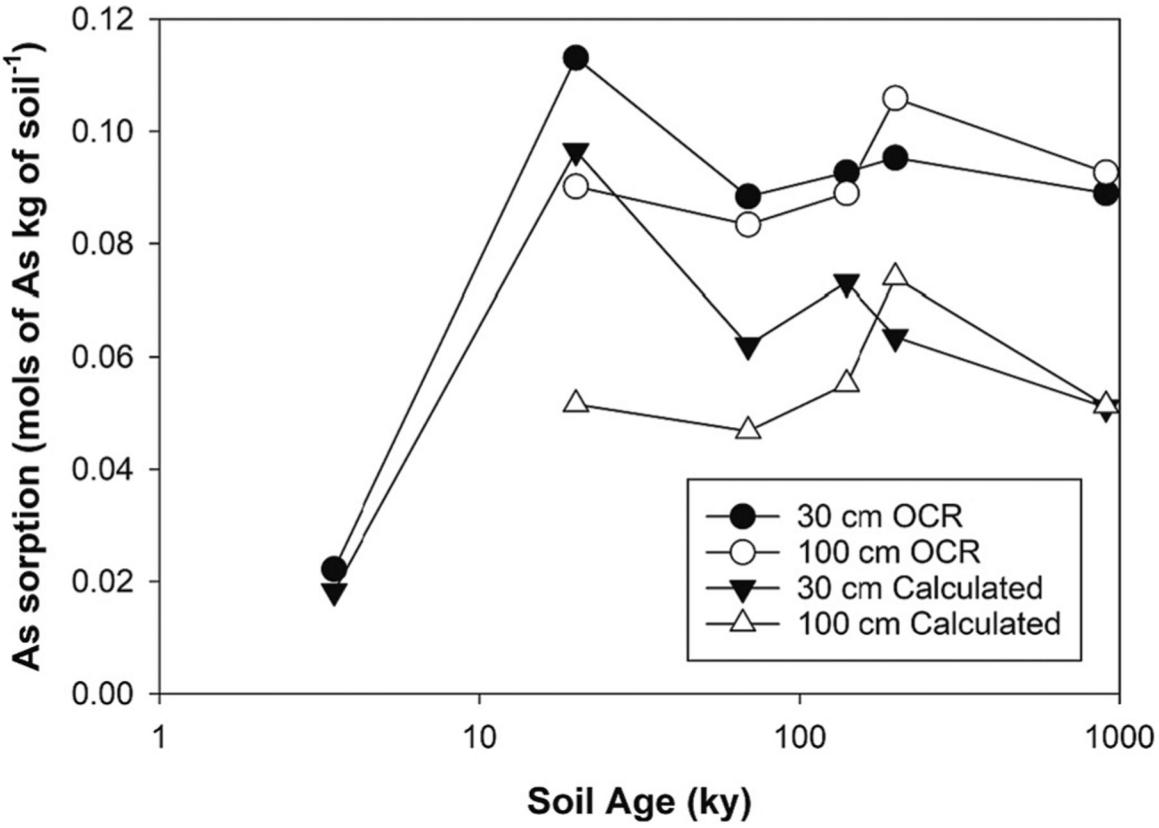

Fig. 8.

Actual and calculated As sorption onto OCR soils from 30- (black symbols) and 100-cm (white symbols) depths. Actual As sorption capacities (circles) are derived from sorption isotherm data and is also presented in Fig. 3. Calculated As sorption capacities (triangles) were calculated using literature As (V) sorption values for ferrihydrite, allophane, goethite, and gibbsite and are based on concentration of Feo, Alo, Fed, and Ald that was presented in Lindeburg et al., 2013.

Table 1

Langmuir model parameters calculated from As sorption isotherms for 30-cm-depth soils. q_{max} represents the maximum sorption capacity and K_L is the Langmuir constant.

Terrace Age (ky)	q_{max} (mg kg^{-1})	K_L	R^2
3.5	1666.66	0.0078	0.998
20	8474.58	0.0098	0.995
69	6622.52	0.0113	0.999
140	6944.44	0.0073	0.999
200	7142.86	0.0109	0.995
908	6666.67	0.0080	0.995

Table 2

Langmuir model parameters calculated from As sorption isotherms for 100-cm-depth soils. q_{max} represents the maximum sorption capacity and K_L is the Langmuir constant.

Terrace Age (ky)	q_{max} (mg kg^{-1})	K_L	R^2
20	6756.76	0.0116	0.994
69	6250.00	0.0171	0.998
140	6666.67	0.0228	0.997
200	7936.51	0.0378	0.993
908	6944.44	0.0226	0.997

Table 3

Arsenic sorption capacities of OCR soils compared to estimated amorphous and crystalline Fe and Al sorption capacities calculated from pure mineral isotherms for soils as a function of age and depth.

Sample Name	Dithionite Extractable Fe (mol kg^{-1})	Oxalate Extractable Fe (mol kg^{-1})	Dithionite Extractable Al (mol kg^{-1})	Oxalate Extractable Al (mol kg^{-1})	Calculated As sorption for ferrihydrite and allophane[a] (mol kg^{-1})	Calculated As Sorption for goethite and gibbsite[b] (mol kg^{-1})	Total Calculated As sorption[c] (mol kg^{-1})	OCR q_{max} (As mol kg^{-1})
3.5 ky 30 cm	0.0948	0.0572	0.0667	0.0778	0.0161	0.0023	0.0183	0.0222
20 ky 30 cm	0.4100	0.2238	0.5077	0.5782	0.0852	0.0113	0.0965	0.1131
69 ky 30 cm	0.5210	0.0931	0.4484	0.4151	0.0498	0.0124	0.0621	0.0883
140 ky 30 cm	0.5962	0.1307	0.4225	0.4521	0.0592	0.0140	0.0732	0.0926
200 ky 30 cm	0.8093	0.0948	0.4744	0.3669	0.0461	0.0174	0.0636	0.0953
908 ky 30 cm	0.9668	0.0555	0.3817	0.2668	0.0313	0.0197	0.0510	0.0889
20 ky 100 cm	0.3831	0.1020	0.3039	0.3076	0.0343	0.0125	0.0468	0.0901
s69 ky 100 cm	0.5711	0.0608	0.3113	0.2928	0.0394	0.0157	0.0552	0.0834
140 ky 100 cm	0.7430	0.0895	0.3484	0.2965	0.0510	0.0229	0.0740	0.0889
200 ky 100 cm	1.0760	0.0823	0.3409	0.4521	0.0294	0.0219	0.0513	0.1059
908 ky 100 cm	1.0957	0.0644	0.3298	0.2260	0.0161	0.0023	0.0183	0.0926

[a]Calculated As sorption capacity for oxalate extractable Fe and Al are based on concentrations extracted from OCR soils that are presented in Lindeburg et al., 2013. Pure mineral sorption isotherms of As(V) and ferrihydrite (Raven et al., 1998) or allophane (Arai et al., 2005; Andersen et al 1976) were used to estimate As sorption of amorphous oxides.

[b]Calculated As sorption capacity for dithionite extractable Fe and Al are based on concentrations extracted from OCR soils that are presented in Lindeburg et al., 2013. Pure mineral sorption isotherms of As(V) and goethite (Grafe et al., 2001) or gibbsite (Ladiera et al 2004) were used to estimate As sorption of crystalline oxides.

[c]Calculated sorption capacities are the sum of predicted As(V) sorption onto ferrihydrite, allophane, goethite, and gibbsite.